c/a Glaser

RF-energy absorption by biological models: calculations based on geometrical optics

Submitted to 1978 Special Supplement to Radio Science

G. I. Rowlandson

Department of Bioengineering

University of Utah, Salt Lake City, Utah 84112

and

P. W. Barber

Departments of Bioengineering and Electrical Engineering

University of Utah, Salt Lake City, Utah 84112

URSI Helsinki ?

RF-Energy Absorption by Biological Models: Calculations Based on Geometrical Optics

G. I. Rowlandson and P. W. Barber

ABSTRACT

Present theoretical calculations to determine the power absorption characteristics of man have failed to obtain numerical results much beyond the first absorption peak (resonance). Current efforts are directed towards better definition of postresonance whole-body absorption. A geometrical optics method has recently been developed and it is used here to compute the absorption characteristics of a prolate spheroidal man model in the high frequency limit. The technique approximates the surface of the prolate spheroid by small planar subareas. The power transmitted into each subarea is determined, and this transmitted power is assumed to be completely absorbed due to the small depth of penetration of electromagnetic waves into lossy biological bodies in the postresonance region. The total power absorbed is found by summing over all subareas. Validity testing with the Mie theory, in conjunction with consideration of the localization principle of geometrical optics, indicates that this technique is applicable to the man model at frequencies of 6 GHz and above. Computer generated results for a 70-kg prolate spheroidal model of man indicate that (1) the dependence of the power absorption on the incident wave polarization and angle of incidence is markedly different from the behavior seen at lower frequencies, (2) the power absorption increases with frequency in the asymptotic limit, and (3) the use of simple planar models is inadequate in determining the absorption characteristics of biological bodies at high frequencies.

INTRODUCTION

There is presently a great interest in the electromagnetic power absorption characteristics of man and animals. This interest is the result of recent concerns about the possible hazardous effects of this form of nonionizing radiation as well as indications that beneficial medical applications are possible. Theoretical calculations play a crucial role in these investigations. The understandable reluctance to use human beings in experiments has necessitated the use of several species of animals in laboratory power absorption studies. Analytic results complement this experimental research in that the ability to theoretically predict the absorption characteristics of biological models aids in experimental design as well as permitting the extrapolation of animal results to man's body configuration.

Early theoretical calculations of whole-body absorption used spherical models, employing the well-known Mie theory for solution. More recently, a long-wavelength approximation has been used to obtain preresonance (resonance is defined as the condition of maximum absorption) results for homogeneous prolate spheroidal and ellipsoidal models [Massoudi et al., 1977]. In the resonance and postresonance frequency ranges, the Extended Boundary Condition Method [Barber, 1977] has been used for homogeneous prolate spheroidal models, while a tensor integral equation technique has been used to analyze irregularly shaped heterogeneous models constructed of cubical subvolumes [Guru et al., 1976].

In all of these methods, one of the goals is to find the average power absorption (usually specified in W/kg) as a function of frequency to as high a frequency as possible for different cases of polarization and orientation of

the incident wave. The long-wavelength method is inherently limited to low frequencies while the other two methods, which both require a numerical solution by digital computer, have an upper frequency limit determined by machine parameters such as core storage and precision. It is clear that new approaches to determining the power absorption characteristics of biological models at the high end of the frequency spectrum must be found.

Geometrical optics methods have been used extensively to obtain asymptotic high-frequency solutions for scattering and diffraction problems [Keller et al., 1956; Keller, 1962]. In this paper a geometrical optics method is used to determine high-frequency power absorption in homogeneous prolate spheroidal biological models. The method is applicable to high-loss dielectric bodies whose physical dimensions are compatible with the "localization principle" [Liou et al., 1971; Born and Wolf, 1964]; i.e., the dimensions of the object allow for the assumption that the incident radiation consists of separate localized rays which intersect the object on planar surfaces. The method becomes increasingly accurate as the size/wavelength ratio and the radius of curvature approach infinity. Computer calculations using this method provide high frequency numerical results to which lower frequency power absorption results can be connected.

METHODOLOGY

Briefly, the technique requires division of the surface of the prolate spheroid into small planar subareas, calculating the area and defining a unit normal vector for each area segment, and then using this information to determine the angle of incidence and the values of the parallel and perpendicular

components of the incident radiation with respect to the plane of incidence for each subarea. Transmission coefficients for each component are then determined. The power transmitted into each subarea is then calculated and assumed to be completely absorbed due to the small depth of penetration of biological tissues at higher frequencies. The total power absorbed by the prolate spheroid is found by summing the transmitted power over all subareas.

The initial step of dividing the surface of the prolate spheroid into small planar subareas is handled by setting up a grid on the surface. This grid is formed by the intersection of two sets of curved lines defined by equal

FIG. 1 angular increments of the spherical coordinate angles θ and ϕ as shown in Fig. 1. Such a grid results in triangular area segments at the poles and trapezoidal segments elsewhere. For small increments in θ and ϕ, the area segments can be assumed to be planar. Once the area segments have been defined, then the interaction of the incident wave with each segment must be determined. This analysis requires that a unit normal and numerical area be determined for each segment. The unit normals are obtained from the gradient of the surface of the prolate spheroid at the midpoint of the planar area segments. Calculated values of the areas are formulated by the values of the angles that subtend them and the size of the prolate spheroid. These parameters enable a calculation of the interaction of the incident radiation with each planar area segment.

The orientation of the unit normals are analyzed with respect to the incident wave, which is defined to lie in the x-z plane (see Fig. 1). The propagation vector of the incident wave is given by:

$$\bar{a}_k = \sin \alpha \, \bar{a}_x + \cos \alpha \, \bar{a}_z \qquad (1)$$

where α is the polar angle from the z-axis towards the positive x-axis. The two polarizations of the incident wave are represented by the unit vectors $\bar{e}_1$ and $\bar{e}_2$, with $\bar{e}_1$ being parallel to the plane defined by the major axis of the prolate spheroid and the $\bar{a}_k$ vector, while $\bar{e}_2$ is perpendicular to this plane. These are represented as follows:

$$\bar{e}_1 = -\cos \alpha \, \bar{a}_x + \sin \alpha \, \bar{a}_z \tag{2}$$

$$\bar{e}_2 = \bar{a}_y \tag{3}$$

The relation between the propagation vector $\bar{a}_k$ and a unit normal vector $\bar{a}_n$ on a particular segment can be expressed mathematically as:

$$\cos \theta_i = -\bar{a}_n \cdot \bar{a}_k \tag{4}$$

where θ_i is the angle of incidence on the subarea. The angle of transmission is found from Snell's law [Born and Wolf, 1964] and the angle of incidence:

$$\sin \theta_t = \frac{\sin \theta_i}{(\varepsilon' - j\varepsilon'')^{1/2}} \tag{5}$$

where $\varepsilon_r = \varepsilon' - j\varepsilon''$ is the complex dielectric constant of the biological tissue. These angles are then utilized in calculating the reflection coefficients for the subarea.

Each subarea has two reflection coefficients [Meyer-Arendt, 1972; Renx et al., 1967]. One is for the component of the incident electric field which is parallel to the plane of incidence. (The plane of incidence is defined as the plane in which the normal unit vector and propagation vector lie.) This

is given by:

$$\Gamma_{\parallel} = \frac{\cos\theta_t/(\varepsilon' - j\varepsilon'')^{1/2} - \cos\theta_i}{\cos\theta_t/(\varepsilon' - j\varepsilon'')^{1/2} + \cos\theta_i} \tag{6}$$

The other reflection coefficient pertains to the component of the incident electric field which is perpendicular to the plane of incidence. The coefficient is:

$$\Gamma_{\perp} = \frac{\sec\theta_t/(\varepsilon' - j\varepsilon'')^{1/2} - \sec\theta_i}{\sec\theta_t/(\varepsilon' - j\varepsilon'')^{1/2} + \sec\theta_i} \tag{7}$$

These are then used to calculate the power transmission coefficients for each subarea, which are $\left(1 - |\Gamma_{\parallel}|^2\right)$ and $\left(1 - |\Gamma_{\perp}|^2\right)$.

To implement these coefficients in the proper manner, the incident electric field must be broken up into two components for each subarea: one parallel to the plane of incidence and one perpendicular to this plane. A convenient method of finding these components of the incident electric field is to define a unit vector perpendicular to the plane of incidence on each subarea and then find components of the incident wave polarization vector which are parallel and perpendicular to this vector. A unit vector perpendicular to the plane of incidence is:

$$\bar{a}_m = -\frac{\bar{a}_n \times \bar{a}_k}{\sin\theta_i} \tag{8}$$

Considering the $\bar{e}_1$ incident wave, the fractional component of $\bar{e}_1$ which is perpendicular to the plane of incidence on a particular subarea is $\bar{e}_1 \cdot \bar{a}_m$.

The fraction of power in this plane is $\left(\bar{e}_1 \cdot \bar{a}_m\right)^2$, and the fraction of incident power parallel to the plane of incidence is $1 - \left(\bar{e}_1 \cdot \bar{a}_m\right)^2$. The total power transmitted into the subarea due to the $\bar{e}_1$ polarized incident wave is then found by multiplying the two fractional components of the incident power by the appropriate power transmission coefficients, the projected area A_p, and the incident power density S_i.

$$P_1 = S_i A_p \left[\left(\bar{e}_1 \cdot \bar{a}_m\right)^2 \left(1 - |\Gamma_\perp|^2\right) + \left(1 - \left(\bar{e}_1 \cdot \bar{a}_m\right)^2\right) \left(1 - |\Gamma_\parallel|^2\right)\right] \quad (9)$$

The projected area A_p is the area of the subarea times cos θ_i. The corresponding expression for the power transmitted due to the $\bar{e}_2$ incident wave is found from the above expression with $\bar{e}_2$ substituted for $\bar{e}_1$. This, then, delineates the interaction that the incident radiation has with the planar subareas.

The total power absorbed by the prolate spheroid is calculated by summing over all subareas and assuming that all of the power transmitted into the prolate spheroid is totally absorbed. This is not a tenuous assumption. Hodkinson, et al. [1963] found that for spherical particles with moderate absorption coefficients, i.e., with $\varepsilon''/\left[\varepsilon' + \left(\varepsilon'^2 + \varepsilon''^2\right)^{1/2}\right] > .1$ and diameters larger than four wavelengths, internally refracted rays may be neglected. Furthermore, Liou, et al. [1971], in studying the scattering by transparent particles, found that only three internal reflections were needed to account for 99 percent of the scattered energy. This, in addition to the fact that at 6 GHz biological tissue has a depth of penetration of 2.6 mm (and at 140 GHz less than 0.5 mm), makes the calculation of the total absorbed power being equal to the summation of all transmitted powers into the subareas appear valid.

VALIDITY TESTING

The equations necessary for the solution of this problem have been programmed on a digital computer. The calculation for a particular prolate spheroidal model is successively repeated for an increasing number of subareas until convergence of the final result is achieved.

Extensive validity testing of the technique was performed by comparing the calculations for spheres with those obtained via Mie theory [Hodkinson et al., 1963; Kerker, 1969]. Correspondence within 10 percent was considered the point at which the geometrical optics technique became valid.

FIG. 2 Figure 2 displays the results of this validity testing by relating the valid frequency in GHz to the radius of the spherical muscle tissue model tested. It can be seen that at 14 GHz the geometrical optics technique can be used to calculate the absorption characteristics of a spherical muscle model of man (radius = 0.256 m) with a confidence of 10 percent.

Although the relationship between valid frequency and sphere size is a straight line on this log-log scale, the slope is not minus one and therefore the relationship cannot be expressed by a constant value of ka ($2\pi a/\lambda$) as might be expected. A curve of constant ka (slope = minus one) is shown in Fig. 2 for comparison.

The reason that the validity criterion cannot be described by a constant ka value has to do with the frequency dispersion of the permittivity and conductivity of muscle tissue. For example, for a constant ka value, calculations for two spheres with different radii must be made at two different frequencies, which therefore requires the use of different dielectric characteristics.

FIG. 3 Figure 3 compares absorption calculations for two muscle spheres using

both Mie theory and geometrical optics approaches. Note particularly the unique resonance characteristics of the two spheres which are caused by the dispersion of the dielectric characteristics. It can be seen that the resonance characteristics of a lossy sphere are greatly influenced by the dielectric characteristics. The geometrical optics calculation cannot account for resonance behavior and therefore deviations between the two methods occur at lower frequencies and these deviations occur at different rates for different spheres, which accounts for the nonconstant ka value for applicability of the geometrical optics approach. Furthermore, since the larger spheres acquire valid solutions more gradually, different slopes of valid ka are obtained for 10 and 20 percent convergence as indicated in Fig. 4.

FIG. 4

Extension of this technique to other models requires that the local radius of curvature and overall size of the model be much greater than a wavelength. For a sphere these conditions are satisfied simultaneously. In the case of the prolate spheroid, the second condition is automatically satisfied if the first condition is met. For a prolate spheroidal model of man (height 1.75 m, width 0.276 m), the minimum radius of curvature is 0.0218 m. From Fig. 2 this minimum radius of curvature indicates that geometrical optics calculations should be computed at a minimum frequency of 130 GHz in order to obtain an accuracy of 10 percent. To restrict calculations for the man-sized prolate spheroid to this high frequency would be an exceedingly stringent criterion, for the minimum radius of curvature occurs at the poles of the spheroid, an area that receives only grazing incident radiation when $\alpha = 90°$. Furthermore, much of the surface of the prolate spheroid approximates a planar surface. (The maximum local radius of curvature at the equator of the prolate

spheroid is 5.548 m.) Therefore, an intermediate value for the minimum radius of curvature would seem more logical as the limiting criterion for extension of this technique to the prolate spheroid. A reasonable value is the dimension b (= 0.138 m), the local minimum radius of curvature at the equator of the prolate spheroid. From Fig. 2, calculations using this dimension as the criterion give a minimum valid frequency of 27 GHz (for 10 percent convergence) and could be said to fulfill the localization principle at the equator. Using larger radii than the b dimension would result in the localization principle not being adequately fulfilled anywhere on the surface of the spheroid. For other prolate spheroidal models, a similar analysis may be done to find the frequency of appropriate applicability.

NUMERICAL RESULTS

Geometrical optics power absorption calculations have been made for a number of biological models. Figure 5 shows the absorption characteristics of a 70 kg prolate spheroidal man model. The lower frequency results were obtained via the Extended Boundary Condition Method [Barber, 1977] while the results at the higher frequencies were obtained by the geometrical optics analysis described here.

FIG. 5

Before discussing the results, a word should be said about the dielectric characteristics that were used in making the calculations. The lower frequency Extended Boundary Condition calculations use dielectric constants and conductivities suitable for tissue consisting of a homogeneous mixture of muscle, fat, and bone. Volume averaging the different tissues of man indicates that these values should be two-thirds those of muscle tissue [Rowlandson, 1977]. This two-

thirds value is appropriate at the lower frequencies where the depth of penetration is large and the electromagnetic interaction occurs throughout the volume of the prolate spheroidal model. At the higher frequencies, however, the depth of penetration is small and the total interaction occurs close to the surface. (The depth of penetration is only a few millimeters for the lowest frequency for which calculations have been made.) At these higher frequencies, electrical characteristics corresponding to skin tissue have been used. Specifically, skin is a high-water-content tissue and the dielectric characteristics can be obtained from high frequency muscle tissue expressions based on the Debye theory for electrically polarizable molecules [Weil, 1975]:

$$\varepsilon' = 5\left[\frac{12 + (f/20)^2}{1 + (f/20)^2}\right] \tag{10}$$

and

$$\sigma = \left[\frac{1 + 62\ (f/20)^2}{1 + (f/20)^2}\right] \text{ mho/m} \tag{11}$$

where f is in GHz. These expressions were multiplied by factors (ε' (0.814), σ (0.78)) in order to obtain better results in agreement with lower frequency muscle tissue data.

It is interesting to note that in the intermediate frequency range, recent work has shown that the skin-fat-muscle layers at the surface play a major role in whole-body absorption and while homogeneous models can be used at low and high frequencies, accurate calculations at intermediate frequencies require an inhomogeneous model.

The E, H, K notation in Fig. 5 refers to the fact that E and H represent

the wave in Fig. 1 incident at an angle of ninety degrees, with E corresponding to the $\bar{e}_1$ incident case and H to the $\bar{e}_2$ case. The K case is for the wave incident at zero degrees. Note that relaxing the convergence criteria allows calculations to be made down to 6 GHz.

These results indicate that biological bodies have moderate to high absorption characteristics at the higher frequencies. Also, there is a reversal in the power absorption characteristics of the different incident waves between the lower and higher frequencies. At lower frequencies, a quasi-static analysis based on the boundary conditions at the surface and eddy-current considerations has shown that the E incident wave is strongly coupled into the spheroid, with progressively weaker coupling by the K and H incident waves [Durney et al., 1975]. In the high-frequency geometrical optics limit, the relative coupling can be analyzed from a surface reflection coefficient standpoint. The E incident wave has an electric field component which is generally perpendicular to the incident plane of the subareas while the H incident wave has an electric field component which is generally parallel to the incident plane. The reflection coefficient for perpendicular electric field components is greater [Meyer-Arendt, 1972], thereby giving less transmitted power for the E wave than the H wave. The K incident wave impinges on most of the subareas at incident angles close to ninety degrees, and therefore most of the incident wave is reflected giving lower absorption. This reversal of power absorption characteristics at the higher frequencies has been confirmed experimentally [Gandhi et al., 1977]. Furthermore, these results indicate that the decline in complex dielectric with frequency produces lower surface reflection coefficients and subsequently greater absorption at the frequency increases. Massoudi, et al. [1977], also encountered this in

implementing his infinite cylinder model. His results are within 4 percent of the results in Fig. 5 for E and H polarizations.

High frequency calculations have been made using planar models to see how well they compare to these geometrical optics results. It was found that the results using a planar model are too large, with some being more than 100 percent too large as compared to the prolate spheroidal model. The reason for this discrepancy is that the planar model does not take into consideration the sharp decrease in transmitted power which occurs when the local angle of incidence is not normal to the surface.

CONCLUSIONS

A method has been outlined, which is based on geometrical optics, that enables calculation of the power absorption characteristics of prolate spheroidal models of biological bodies at the high end of the frequency spectrum. The primary use of these results is that they provide asymptotes to which previously calculated low-frequency results can be connected. The technique has been validity tested through comparison of calculations for spheres from the Mie theory.

Calculations for a prolate spheroidal model of man using the b dimension of the spheroid as the limiting radius of curvature have permitted calculations down to 6 GHz for the man model. These results are expected to be accurate within 20 percent. The results from this prolate spheroidal model indicate that (1) the maximum power is deposited by the H incident wave, with decreasing absorption due to E and K waves, a reversal of the behavior seen at lower frequencies, (2) due to the decrease in permittivity with increasing

frequency, which effectively results in a better impedance match between the model and surrounding free space, biological bodies experience increasing absorption as the frequency increases, and (3) the use of simple planar models is inadequate in calculating the absorption characteristics of biological bodies.

ACKNOWLEDGMENTS

This work was supported by the USAF School of Aerospace Medicine, Brooks Air Force Base, Texas 78235. The authors would like to thank Professor Carl H. Durney for his constructive comments during the preparation of this paper.

REFERENCES

Barber, P., Electromagnetic power absorption in prolate spheroidal models of man and animals at resonance, to appear in *IEEE Trans. Biomed. Eng.*

Born, M., and E. Wolf (1964), *Principles of Optics*, pp. 109-125, Macmillan, New York.

Durney, C. H., C. C. Johnson, and H. Massoudi (1975), Long wavelength electromagnetic power absorption in prolate spheroid models of man and animals, *IEEE Trans. Microwave Theory Tech.*, MTT-23, 739-747.

Gandhi, O. P., and E. L. Hunt, Deposition of electromagnetic energy, submitted to *IEEE Trans. Microwave Theory Tech.*

Guru, B. S., and K. M. Chen (1976), Experimental and theoretical studies on electromagnetic fields induced inside finite biological bodies, *IEEE Trans. Microwave Theory Tech.*, MTT-24, 433-440.

Hodkinson, J. R., and I. Greenleaves (1963), Computation of light scattering and extinction by spheres according to diffraction and geometrical optics, and some comparisons with Mie theory, *J. Opt. Soc. Amer.*, 53, 577-588.

Keller, J. B. (1962), Geometrical theory of diffraction, *J. Opt. Soc. Amer.*, 52, 116-130.

Keller, Lewis, and Seckler (1956), Asymptotic solutions of some diffraction problems, *Comm. Pure Appl. Math.*, 9, 207-265.

Kerker, M. (1969), *The Scattering of Light and Other Electromagnetic Radiation*, pp. 27-97, Academic, New York.

Liou, K., and J. E. Hansen (1971), Intensity and polarization for single scattering by poly disperse sphere: a comparison of ray optics and Mie theory, *J. Atmos. Sci.*, 28, 995-1004.

Massoudi, H., C. H. Durney, and C. C. Johnson (1977), Long wavelength electromagnetic power absorption in ellipsoidal models of man and animals, *IEEE Trans. Microwave Theory Tech.*, MTT-24, 41-47.

Massoudi, H., C. H. Durney, and C. C. Johnson, The geometrical optics and exact solution for internal fields and SAR in a cylindrical model of man irradiated by an electromagnetic plane wave, submitted to 1978 special supplement to *Radio Science*.

Meyer-Arendt, J. R. (1972), *Introduction to Classical and Modern Optics*, pp. 280-320, Prentice-Hall, Englewood Cliffs, New Jersey.

Renx, J. R., and F. J. Milford (1967), *Foundations of Electromagnetic Theory*, pp. 300-340, Addison-Wesley, London.

Weil, C. M. (1975), Absorption characteristics of multilayered sphere models exposed to UHF/microwave radiation, *IEEE Trans. Biomed. Eng.*, BME-22 468-476.

FIGURE CAPTIONS

1. Orientation of the prolate spheroid and an individual subarea with respect to the incident wave.
2. Valid frequency (10 percent convergence criteria) versus radius of spherical muscle model. The dashed line of constant ka is for comparison.
3. Convergence testing results for two different muscle spheres showing the frequencies of 10 percent and 20 percent convergence.
4. ka versus sphere radius for 10 percent and 20 percent convergence criteria.
5. SAR in a 70-kg prolate spheroidal man model for an incident power density of 1 mW/cm^2. Height = 1.75 m, height/width = 6.34. Relaxing the convergence criteria to 20 percent (based on the minimum radius of curvature at the equator) permits calculations down to 6 GHz.

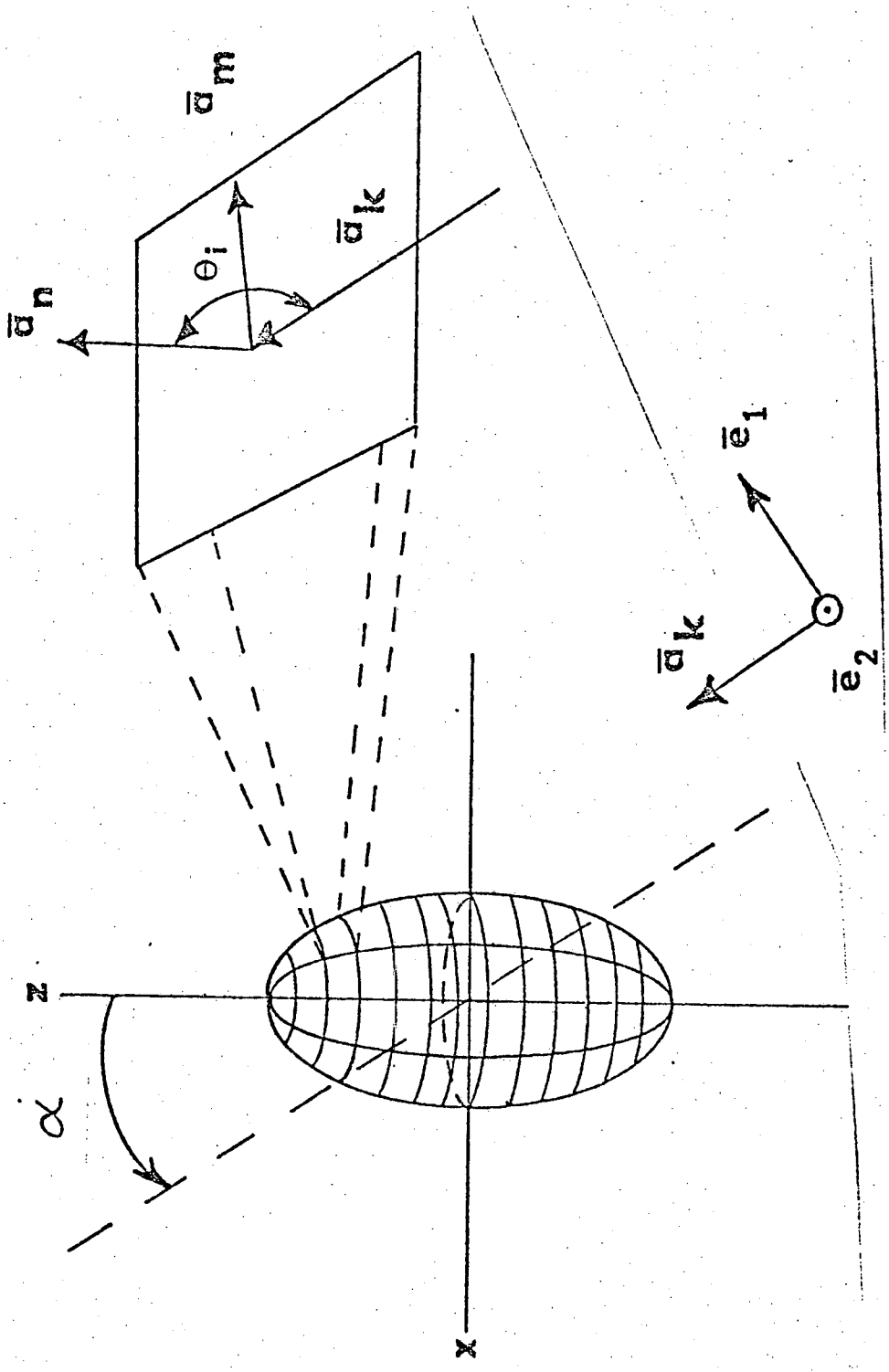

Fig. 1

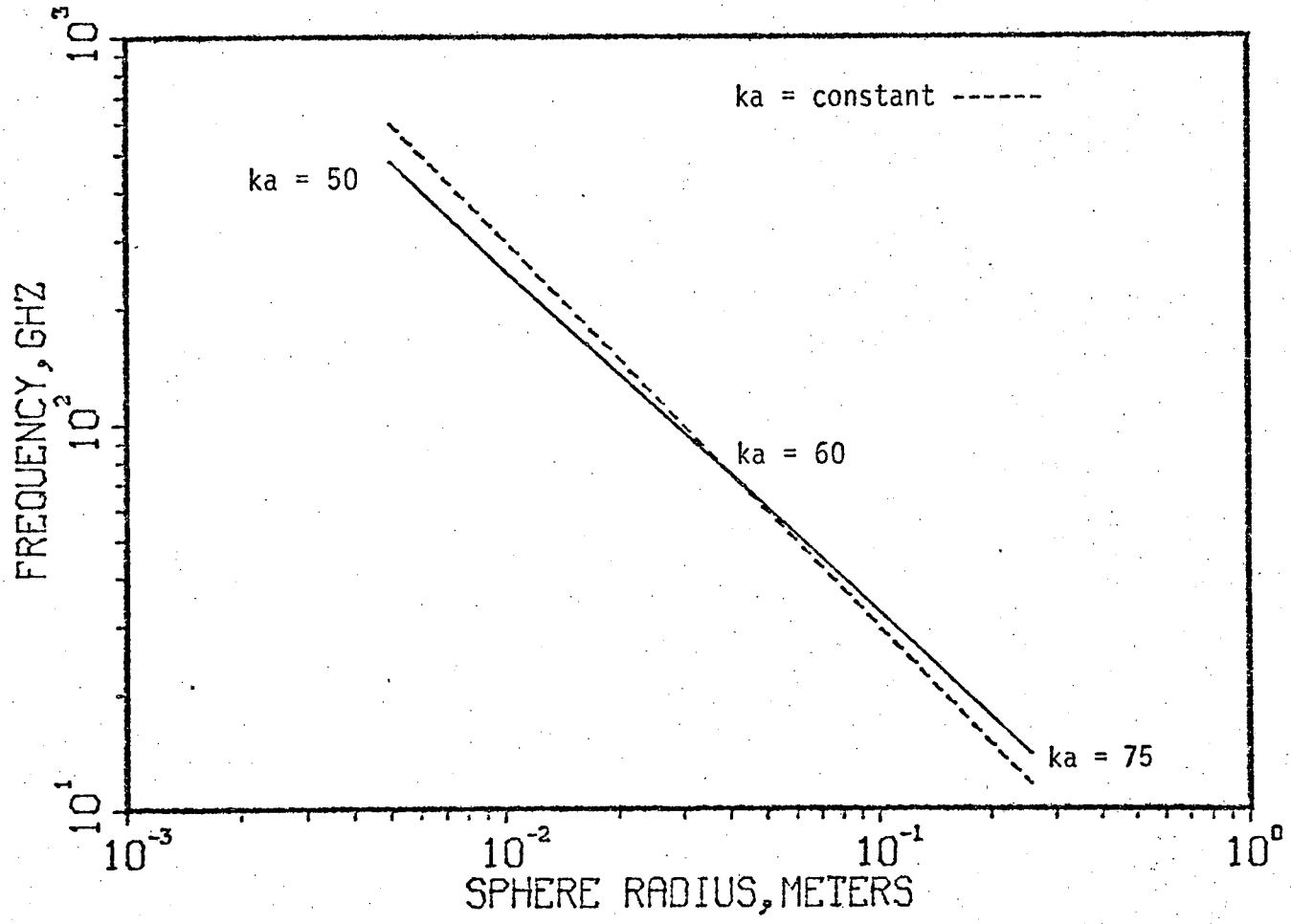
ka = constant ------
ka = 50
ka = 60
ka = 75
FREQUENCY, GHZ
10^3
10^2
10^1
10^{-3}
10^{-2}
10^{-1}
10^0
SPHERE RADIUS, METERS

Figure 2

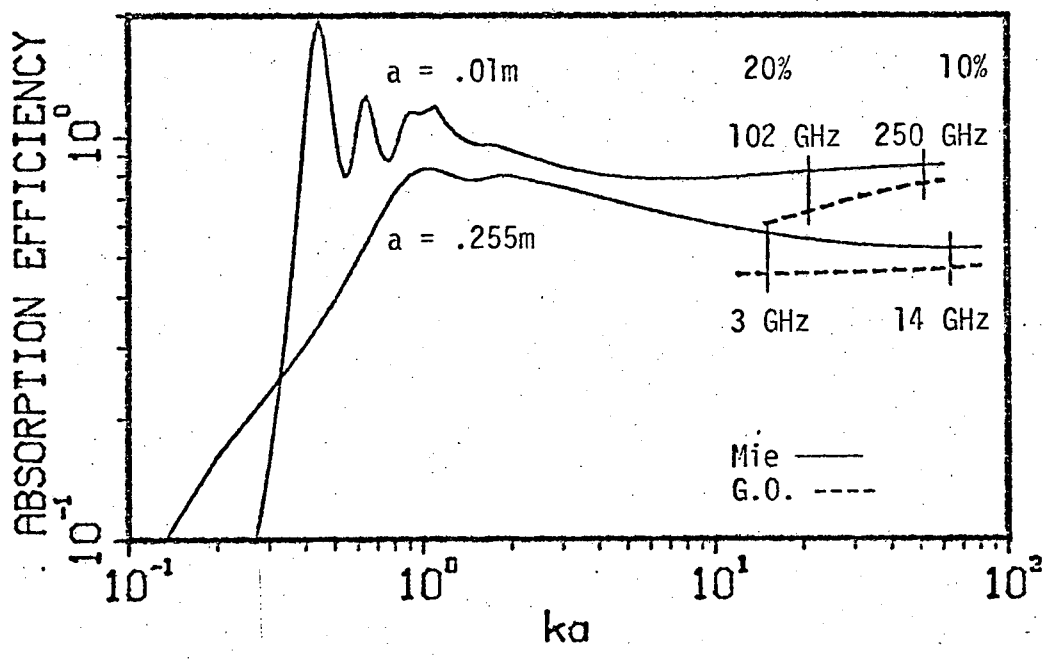
ABSORPTION EFFICIENCY
10^0
10^{-1}
a = .01m
a = .255m
20%
10%
102 GHz
250 GHz
3 GHz
14 GHz
Mie
G.O.
10^{-1}
10^0
10^1
10^2
ka

Fig. 3

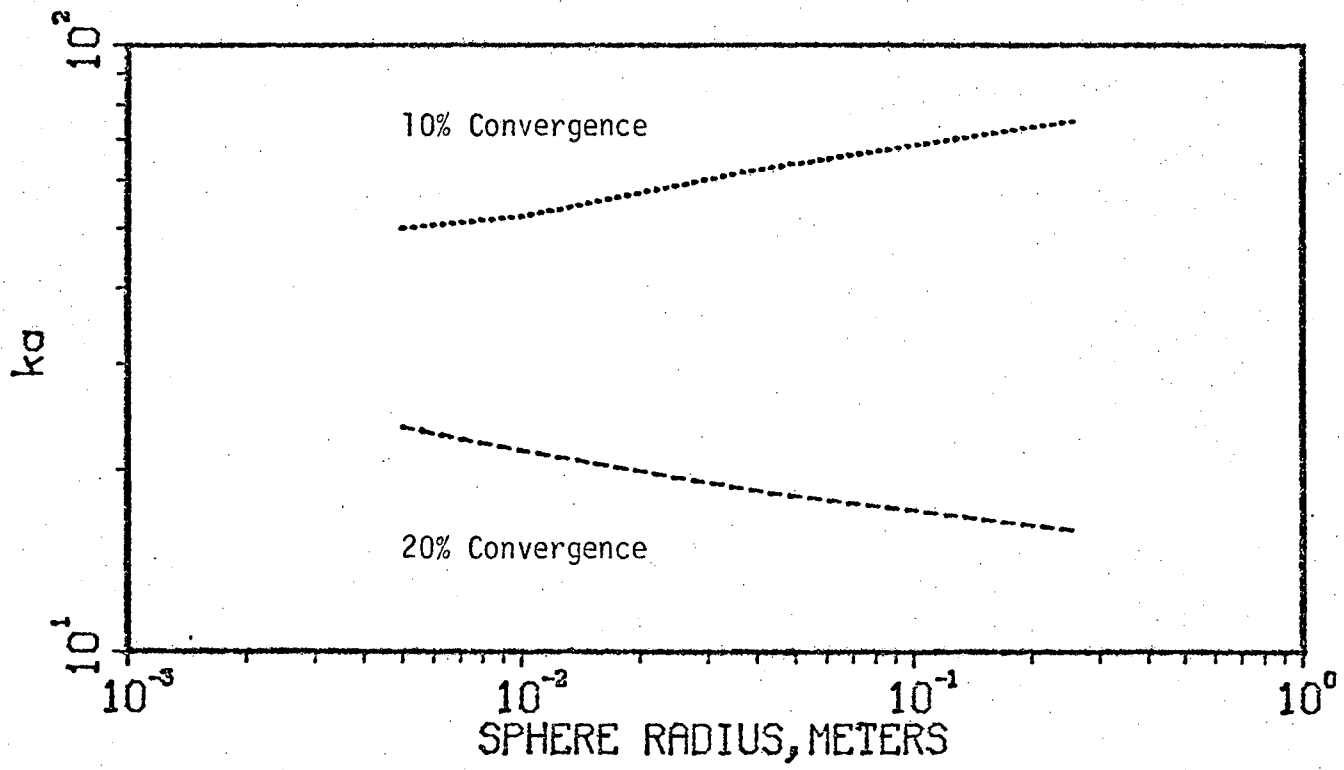
10^2
10^1
ka
10% Convergence
20% Convergence
10^{-3}
10^{-2}
10^{-1}
10^0
SPHERE RADIUS, METERS

Figure 4

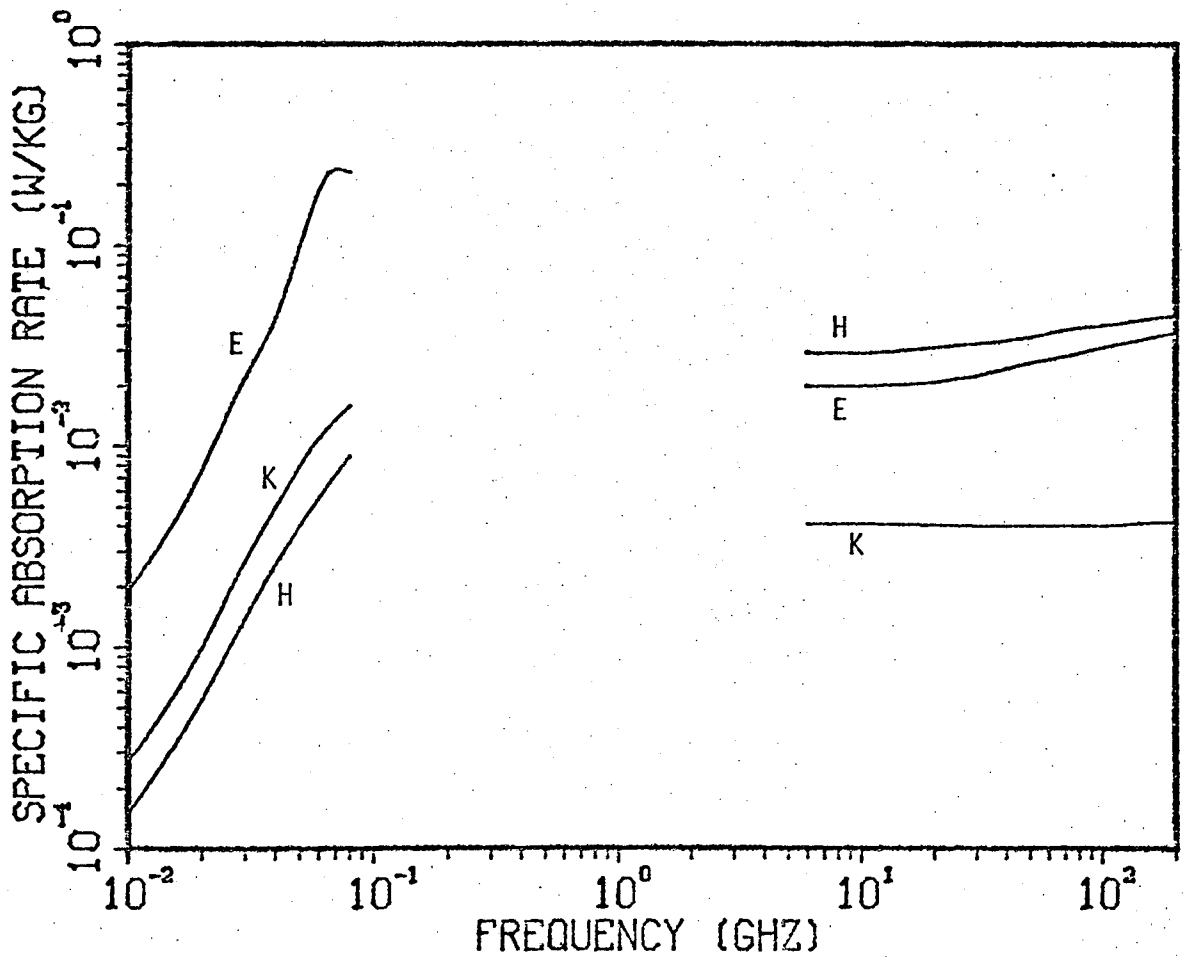
SPECIFIC ABSORPTION RATE (W/KG)
10^{0}
10^{-1}
10^{-2}
10^{-3}
10^{-4}
E
K
H
H
E
K
10^{-2}
10^{-1}
10^{0}
10^{1}
10^{2}
FREQUENCY (GHZ)

Fig. 5